Nanoscale Research Letters

NANO EXPRESS Open Access

New Insights on Factors Limiting the Carrier Transport in Very Thin Amorphous Sn-Doped In_2O_3 Films with High Hall Mobility

Yutaka Furubayashi[1*], Makoto Maehara[2] and Tetsuya Yamamoto[1]

Abstract

We demonstrated that a mass density and size effect are dominant factors to limit the transport properties of very thin amorphous Sn-doped In_2O_3 (*a*-ITO) films. *a*-ITO films with various thicknesses (*t*) ranging from 5 to 50 nm were deposited on non-alkali glass substrates without intentional heating of the substrates by reactive plasma deposition with direct-current arc discharge. *a*-ITO films with *t* of more than 10 nm showed a high Hall mobility (μ_H) of more than 50 cm^2/V s. For 5-nm-thick *a*-ITO films, we found that μ_H was as high as more than 40 cm^2/V s. X-ray reflectivity measurement results revealed that the mass density (d_m) determined the carrier transport in *a*-ITO films. For *a*-ITO films with *t* of more than 10 nm, d_m had a high value of 7.2 g/cm^3, whereas *a*-ITO films with *t* of less than 10 nm had low d_m ranging from 6.6 to 6.8 g/cm^3. Quantitative new insight from a size effect on the carrier transport is given for *a*-ITO films with *t* of less than 10 nm. This study shows that the ratio of *t* to mean free path of carrier electrons governed μ_H.

Keywords: Tin-doped indium oxide, Amorphous film, Hall mobility, Mass density, Mean free path

Introduction

Sn-doped indium oxide (ITO) has been mostly applied to transparent conducting oxide (TCO) films. Indium oxide (In_2O_3) has a bixbyite crystal structure (space group *Ia*-3, number 206), which comprises distorted InO_6 octahedra containing some oxygen defects. This is a periodic structure that produces structural vacancies (V_{str}). Both an oxygen (O) and a structural vacancy are shared between adjacent polyhedra with the result that the polyhedra are joined at a corner occupied by the O, which is referred to as corner sharing hereafter. On the other hand, two O atoms are shared between adjacent polyhedra with the result that the polyhedral are joined along the entire edge, referred to as edge sharing hereafter. The edge-sharing structure allows a large overlap between the wavefunctions of 5*s* and 5*p* orbitals of the valence electrons of In atoms owing to the short interatomic distance of about 0.334 nm between In atoms, which should provide a high carrier mobility [1, 2]. In particular, toward widening the optically transparent range from the visible to the near-infrared spectral region for applications such as solar cells, a high Hall mobility (μ_H) of more than 100 cm^2/V s has recently been reported for hydrogenated [3] and Ce-doped hydrogenated [4] In_2O_3-based polycrystalline TCO films.

Most of the papers on ITO films have focused on their application as TCO films for which the typical thickness (*t*) is more than 50 nm [5]. In fact, because a TCO layer is used as an antireflection layer in a solar cell, *t* is fixed to approximately 75 nm [2]. For this value, the carrier transport properties can be described as those of a bulk material. On the other hand, there are few papers on very thin ITO films with *t* of less than 50 nm because thinner TCO films have a high electrical sheet resistance, making them unsuitable for applications. Shigesato et al. reported the electrical properties of very thin amorphous-phase ITO (*a*-ITO) films deposited by sputtering at the initial stage of growth [6]. The maximum

* Correspondence: furubayashi.yutaka@kochi-tech.ac.jp
[1]Materials Design Center, Kochi University of Technology, Tosayamadacho-Miyanokuchi 185, Kami 782-8502, Japan
Full list of author information is available at the end of the article

μ_H was 40 cm^2/V s for *a*-ITO films with *t* of 20 nm, and there was an abrupt decrease in μ_H with decreasing *t*. The initial stage of the growth of films deposited by pulsed-laser deposition (PLD) was also reported [7], where the article focused on the critical thickness and the detailed transport mechanism was not discussed.

The scattering mechanisms which include grain boundary and intragrain scattering mechanism originated by various scattering centers such as phonons, ionized impurities, and neutral impurities have been discussed for degenerated polycrystalline ITO films [8]. In contrast, for *a*-ITO films with no grain boundaries, the randomness of the In–O polyhedral-based network with short-range order should be taken into account. A preliminary analysis of amorphous zinc-doped In_2O_3 (*a*-IZO) films was reported [9] that was based on a defect model [10]. Utsuno et al. investigated the bonding states of both *a*- and crystalized In_2O_3 by a simulation analysis of grazing incidence X-ray scattering [11]. Buchholz et al. focused on the mass density of *a*-In_2O_3 films [12]. However, a comprehensive understanding of the dominant factors limiting carrier transport in *a*-In_2O_3-related systems, particularly very thin films, is still lacking because there has been no report directly showing the origin of the scattering factors.

In this work, we used ion plating with direct-current (DC) arc discharge of which product name is reactive plasma deposition (RPD) that has been commercially employed [13]. RPD with a high growth rate [14, 15] enables the fabrication of films with a uniform spatial distribution of *t* prepared on large substrates with a size such as 1.5 × 1.5 m^2. In addition, we have recently fabricated a dense ZnO film with a thickness of 10 nm [16]. The use of RPD is thus expected to enable a reliable study of the carrier transport in very thin *a*-ITO films toward achieving high μ_H TCOs.

In this paper, we report the successful fabrication of very thin TCO films (t < 50 nm) based on *a*-ITO films with a high μ_H by using RPD. We found that the mass density (d_m) is the most important factor for describing the carrier transport properties of the *a*-ITO system. We also reveal the relationship between μ_H and d_m.

Method

ITO films were grown on non-alkali glass substrates (Corning Eagle XG) using RPD apparatus (Sumitomo Heavy Industries, Ltd.) shown in Fig. 1. The exposure of arc plasma of electropositive argon (Ar^+) ions and electrons generated by the pressure gradient Uramoto gun [17] to a source material made from In_2O_3 with a 5 wt.% corresponding to 4.6 at.% content of SnO_2 leads to the sublimation of the source. Subsequently, some of the vaporized atoms such as In, Sn, and O change to electropositive ions such as In^+, Sn^+, and O^+ ions, respectively, as results of the interactions with electrons. The source material pressed with a cylindrical form (height of 40 mm and a diameter of 30 mm) and sintered was used. The flow rates of Ar gas introduced into the deposition chamber and into a plasma gun were 25 and 40 sccm, respectively. The *a*-ITO films with *t* ranging from 5 to 50 nm were fabricated with an oxygen (O_2) gas flow rate (OFR) of 20 or 30 sccm without intentional heating of the substrate (the substrate temperature was of less than 70 °C as a result of arc-plasma exposure). The total pressure during the growth was 0.3 Pa. The typical growth rate was 3.6 nm/s. A thickness *t* was controlled by changing the traveling speed of the substrate [18].

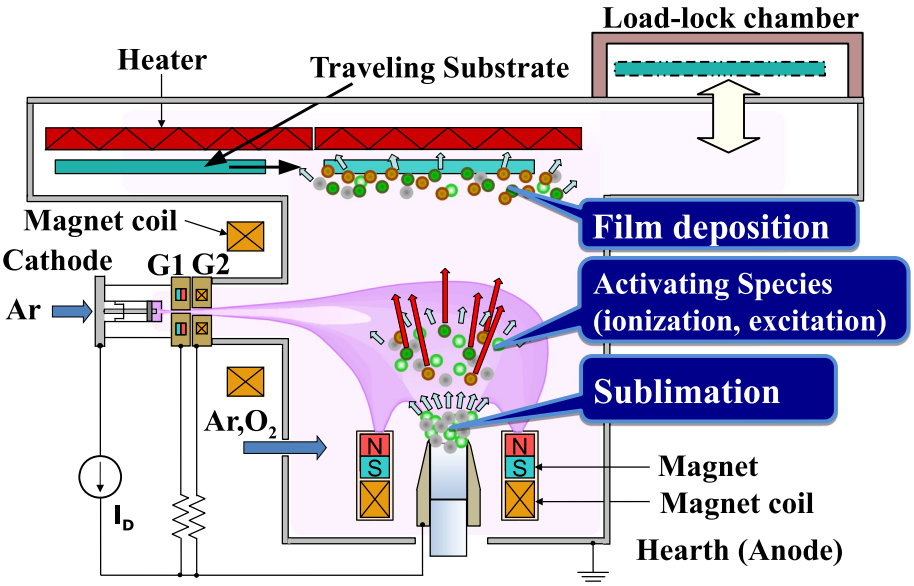

Fig. 1 Schematic diagram of RPD with DC arc discharge

X-ray diffraction (XRD) and X-ray reflectivity (XRR) measurements were performed with a Rigaku ATX-G diffractometer having an X-ray source of Cu-Kα (wavelength of 0.15405 nm) to determine the structural properties of *a*-ITO films. Both XRD and XRR measurements were carried out with the same $2\theta/\omega$ configuration. The roughness and thickness of the samples were evaluated from an analysis of the XRR measurement results. An auxiliary measurement of the thicknesses was performed by using Dektak 6M stylus surface profiler (Bruker Corporation). The electrical properties at room temperature were evaluated in a van der Pauw geometry by using Nanometrics HL5500PC measurement system.

RPD equipment used in this work has been employed as a mass production usage. The spatial uniformity and the reproducibility of physical properties (including transport and thickness) of fabricated films are already ensured within ± 5% [19, 20]. Note that all the data points obtained by single measurements are sufficient in reliability.

Results and Discussion

Mass Density of *a*-ITO Films

No peaks were detected by XRD measurements for all the sample films, which indicates amorphous-phase films. XRR is a powerful and nondestructive technique used to study t and d_m for *a*-ITO films. In this work, t and d_m were estimated by using the XRR measurement results based on a two-layer model with an *a*-ITO film surface and a rough interface (ITO/glass) [12]. Taking into account the fact that d_m derived from the critical angle of an XRR profile corresponds to the mass density near the surface of a film, in this work, we determined d_m values from the amplitude of the oscillation for the total reflection. The results enabled us to study the relationship between d_m and the carrier mobility averaged over the whole films determined by Hall effect measurements.

Figure 2 displays XRR spectra of *a*-ITO films with t of 5.1, 20.9, and 47.6 nm grown at an OFR of 20 sccm. For all the *a*-ITO films, the measured XRR curves were very well fitted by the two-layer model, as shown by the black solid curves in Fig. 2. Table 1 summarizes t, d_m, surface roughness r_s, and interface roughness r_i for *a*-ITO films determined by the XRR measurements. The thickness t of all the ITO films had a good agreement with those estimated by a stylus surface profiler. The values of r_s and r_i were around 1 nm irrespective to t and OFR. Figure 3 also shows d_m with an accuracy of ± 0.1 g/cm^3 [21] as a function of t, which was evaluated from the XRR measurements. The *a*-ITO films with t of more than 10 nm exhibited d_m of about 7.2 g/cm^3, which was almost the same as that of bulk ITO [12]. The d_m for *a*-ITO films with t below 7 nm decreased abruptly with decreasing t regardless of the OFR; the d_m values of 5-nm-thick *a*-ITO films with OFRs of 20 and 30 sccm were 6.6 and 6.8 g/cm^3, respectively.

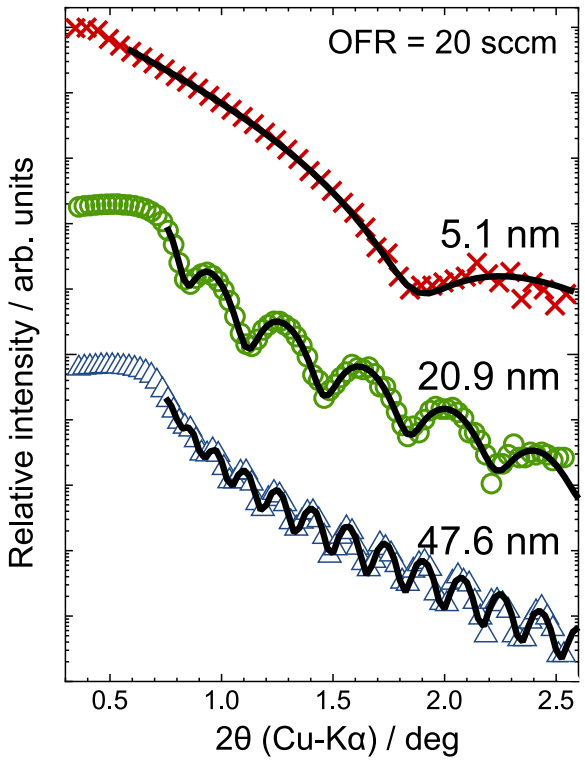

Fig. 2 XRR data (crosses, circles, and triangles) and fitted curves (solid lines) of *a*-ITO films with thicknesses of 5.1, 20.9, and 47.6 nm grown at an OFR of 20 sccm

Table 1 Thickness (t), mass density (d_m), and surface and interface roughness (r_s and r_i, respectively) for *a*-ITO films determined by XRR measurements

Film #	OFR (sccm)	t (nm)	d_m (g cm^{-3})	r_s (nm)	r_i (nm)
1	20	5.12	6.62	0.89	0.92
2		7.14	6.95	0.89	1.04
3		10.3	7.17	0.88	1.04
4		20.9	7.18	0.84	1.06
5		30.0	7.08	0.74	1.06
6		47.6	7.17	0.77	0.90
7	30	5.10	6.76	0.92	0.93
8		7.26	7.13	0.74	0.84
9		10.2	7.08	0.76	0.84
10		20.9	7.19	0.81	1.00
11		30.2	7.15	1.10	1.53
12		49.5	7.13	0.69	0.84

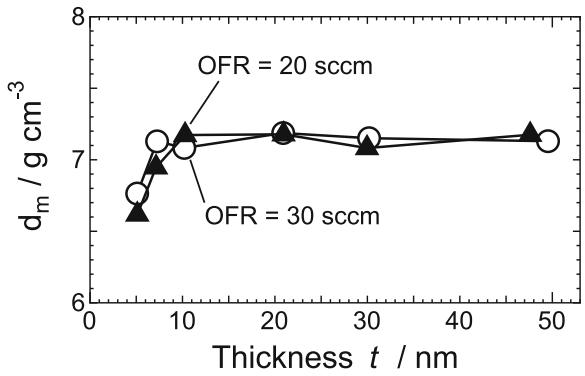

Fig. 3 Mass density d_m derived from XRR measurement results of *a*-ITO films grown at an OFR of 20 sccm (triangles) or 30 sccm (circles) as a function of film thickness *t*

Transport Properties

Figure 4 shows (a) electrical resistivity ρ, (b) carrier density n_e, and (c) μ_H for *a*-ITO films at OFRs of 20 and 30 sccm determined by Hall effect measurements at room temperature. At any given *t*, n_e for *a*-ITO films at an OFR of 20 sccm was larger than that for *a*-ITO films at an OFR of 30 sccm, whereas μ_H for *a*-ITO films at an OFR of 20 sccm was smaller than that for *a*-ITO films at an OFR of 30 sccm. This suggests that the ionized impurity scattering mechanism is one of the factors determining the n_e-dependent μ_H for *a*-ITO films. The above suggested OFR dependence of n_e implies that oxygen vacancies can play a role as donor defects under the following assumptions: (1) the OFR dependence of the residual amount of Sn dopants and of the doping efficiency of the Sn donors is very small compared to the OFR dependence of the density of oxygen vacancies and (2) the density of oxygen vacancies generating shallow donor levels decreases with increasing OFR. Note that for *t* of less than 30 nm, it was found that μ_H increased with n_e, which cannot be explained by conventional ionized scattering. This implies that the carrier transport is governed by another factor, such as a size effect, which will be discussed later, for *a*-ITO films.

In the case of sputtering [6] and PLD [7], the reported critical thickness was 4 nm, where a three-dimensional (3D) process turned out to be dominant and the coalescence of islands was not completed. In such films, μ_H will be significantly small around the critical thickness. For *a*-ITO films deposited by RPD, the relative decrease in μ_H at a *t* of 5 nm was less than 30% compared with that for *a*-ITO films with *t* of more than 10 nm. This suggests that RPD produces ITO films exhibiting growth via a two-dimensional (2D) process, which has already been proved for ZnO films [16].

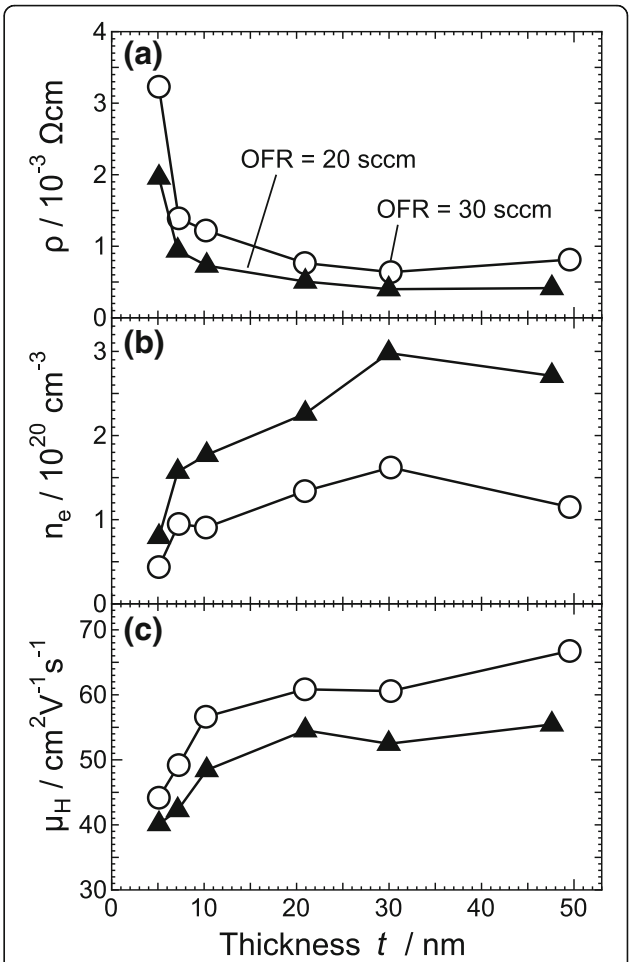

Fig. 4 **a** Electrical resistivity ρ, **b** carrier concentration n_e, and **c** Hall mobility μ_H of *a*-ITO films grown at an OFR of 20 sccm (triangles) or 30 sccm (circles) as functions of thickness *t*. All values were obtained at room temperature

Dominant Features Determing μ_H for the Films: Mass Density and Mean Free Path

Figure 5 shows the dependence of μ_H on d_m for *a*-ITO films at OFRs of 20 and 30 sccm. We found that μ_H and d_m have a strong positive correlation with its high correlation coefficient of 0.73. The results of the analysis of grazing incidence X-ray scattering by simulation suggest that *a*-In_2O_3 has more corner-sharing In–O–In bonds than crystalline In_2O_3 (Fig. 6a) [11, 12, 22]. If we assume that *a*-ITO films also have more corner-sharing In–O–In bonds than crystalline ITO films (see Fig. 6b for the model), the generation of an added vacant defect of an O atom (V_{add}) in two edge-sharing O–O promotes the change in polyhedra from edge sharing to corner sharing. Subsequently, the polyhedra can rotate along an edge, thereby separating adjacent polyhedra, resulting in disjoint corner-sharing polyhedra (see Fig. 6c for the resulting model). This will result in *a*-ITO films with low d_m together with a reduced In–O coordination number, corresponding to the very thin *a*-ITO films

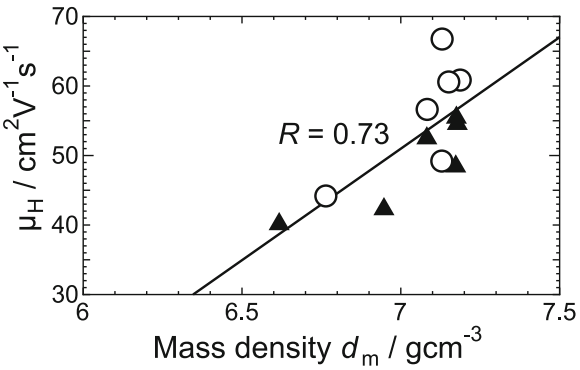

Fig. 5 Relationship between Hall mobility μ_H and mass density d_m of *a*-ITO films grown at an OFR of 20 sccm (triangles) or 30 sccm (circles). The solid line represents a linear fit to all the data with its correlation coefficient *R* specified

with thicknesses of less than 10 nm. In such films, the In–In interatomic distance between the corner-shared In–O polyhedral is increased. This reduces the overlap of the wavefunctions of In valence 5*s* and 5*p* orbitals, resulting in low carrier transport together with the transformation of excess electrons provided by *n*-type defects, such as Sn substituting In atoms and O vacancies, from delocalized to localized states. We confirmed reduced n_e and μ_H for 5-nm-thick *a*-ITO films as respectively shown in Figs. 4b and c. The above discussion combined with the experimental results leads to the conclusion that the carrier transport of *a*-In_2O_3 films is strongly governed by d_m, which determines the proportion of corner-sharing In–O polyhedra.

In addition to the above effect of d_m on carrier transport, the effects of the vertical size, i.e. *t*, on carrier mobility should be taken into account for *a*-ITO films with *t* of less than 10 nm. We estimated the mean free path of carriers (MFP; λ) from the transport properties shown in Fig. 4. On the basis of the Fermi gas model, the Fermi velocity of carriers, v_F, can be written as $v_F = (h/2m^*)(3n_e/\pi)^{1/3}$ [23], where *h* and m^* denote the Planck constant and the effective mass of free electrons, respectively. Using the formula for carrier mobility ($\mu = e\tau/m^*$, where *e* and τ are the elemental charge and scattering time of carriers, respectively), λ can be given by

$$\lambda = v_F\tau = \frac{\mu h}{2e}\left(\frac{3n_e}{\pi}\right)^{1/3}.$$

In this study, we took μ_H as μ and assumed that this model can be adopted for the *a*-ITO films. Figure 7a shows λ as a function of *t*. With increasing *t* up to 10 nm, λ increased sharply. With further increasing *t*, λ increased slowly, then tended to remain almost constant. This behavior of λ did not depend on the OFR owing to the compensation of effects between n_e and μ_H. To clarify the above size effect, μ_H was plotted as a function of

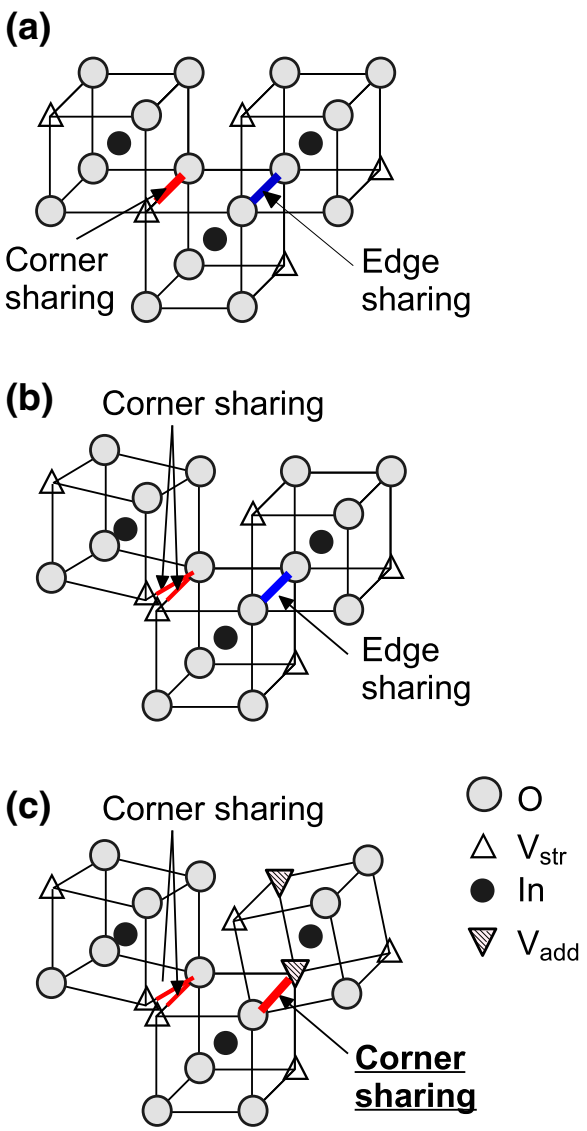

Fig. 6 Models of local structure of **a** crystalline ITO, **b** *a*-ITO, and **c** very thin *a*-ITO with added O vacancy defects (V_{add}), resulting in the transformation from edge sharing to corner sharing

t/λ, in Fig. 7b. This relationship clearly reveals that there is a bending of a slope at $t/\lambda \sim 2$, which corresponds to t = 10 nm. The slope [A] in Fig. 7b is a fitted line for all of the data with $t \leq 10$ nm and those two named [B 20 sccm] and [B 30 sccm] are ones for the data with $t \geq 10$ nm, grown at OFRs of 20 and 30 sccm, respectively. It is obviously seen that those slopes have high correlation coefficients of more than 0.75. This indicates that the dependence of λ on the transport properties of the *a*-ITO films was found to change at *t* of 10 nm. Taking into account the fact that λ is comparable to *t* for very thin *a*-ITO films, we conclude that the reflection of carriers on both the surface and the interface should also be a dominant factor determining μ_H.

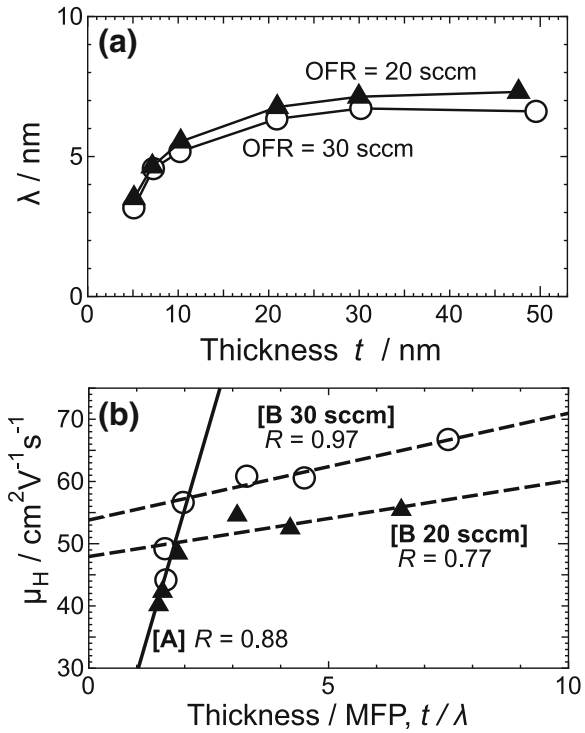

Fig. 7 a Mean free path λ as a function of film thickness t and **b** relationship between Hall mobility μ_H and the ratio of thickness t to λ, t/λ, for a-ITO films grown at an OFR of 20 sccm (triangles) or of 30 sccm (circles). The solid line [A] and dot-dashed line [B; for each OFR] denote linear fits of the data for t = 5–10 nm and t = 10–50 nm, respectively. The correlation coefficients R are specified for all fitted lines

Conclusion

We successfully fabricated very thin a-ITO films with a high μ_H on glass substrates by using RPD. The relatively high d_m together with the high μ_H for a small t suggests almost 2D initial growth. We found that d_m is a dominant factor limiting the carrier transport of the a-ITO system, which is considered to be caused by the existence of corner-sharing In–O polyhedra in a matrix of edge-sharing In–O polyhedra-based network. For a-ITO films with t of less than 10 nm, the properties of the carrier transport can be characterized in terms of both d_m and λ for carriers. On the other hand, for a-ITO films with t of more than 10 nm, the carrier transport can be mainly described within the framework of bulk ITO without the surface or interface scattering of carriers. As the next step, we will determine the lattice structures of a-ITO films with various thicknesses.

Abbreviations

2D: Two dimensional; 3D: Three dimensional; a-In_2O_3: Amorphous-phase indium oxide (III); a-ITO: Amorphous-phase tin-doped indium oxide; a-IZO: Amorphous-phase zinc-doped indium oxide; DC: Direct current; ITO: Tin-doped indium oxide; MFP: Mean free path of carriers; OFR: Oxygen flow rate during deposition; PLD: Pulsed-laser deposition; RPD: Reactive plasma deposition; TCO: Transparent conducting oxide; V_{add}: Added O vacancy defect; V_{str}: Structural vacancy; XRD: X-ray diffraction; XRR: X-ray reflectivity

Acknowledgements

The authors gratefully acknowledge Mr. Toshiyuki Sakemi and Mr. Hisashi Kitami of Sumitomo Heavy Industries, Ltd., for their helpful discussions during this study.

Funding

This study was supported by a collaboration with Sumitomo Heavy Industries, Ltd.

Availability of Data and Materials

The data and the analysis in the current work are available from the corresponding authors on reasonable request.

Authors' Contributions

YF measured XRR and Hall effects of all the ITO samples and wrote the manuscript. YF and TY constructed models determining the factors limiting the carrier transport. MM fabricated all the ITO samples in this study after optimizing the deposition conditions for the film growth. All authors read and approved the final manuscript.

Authors' Information

N/A

Competing Interests

The authors declare that there are no competing interests.

Publisher's Note

Author details

[1]Materials Design Center, Kochi University of Technology, Tosayamadacho-Miyanokuchi 185, Kami 782-8502, Japan. [2]Industrial Equipment Division, Sumitomo Heavy Industries, Ltd., Soubiraki-cho 5-2, Niihama 792-8588, Japan.

Received: 10 December 2018 Accepted: 18 March 2019
Published online: 02 April 2019

References

1. Calnan S, Tiwari AN (2010) High mobility transparent conducting oxides for thin film solar cells. Thin Solid Films 518(7):1839–1849
2. Koida T (2017) Amorphous and crystalline In_2O_3-based transparent conducting films for photovoltaics. Phys Status Solidi A 214(2):1600464
3. Koida T, Fujiwara H, Kondo M (2008) Structural and electrical properties of hydrogen-doped In_2O_3 films fabricated by solid-phase crystallization. J Non-Cryst Solids 354(19-25):2805–2808
4. Kobayashi E, Watabe Y, Yamamoto T (2015) High-mobility transparent conductive thin films of cerium-doped hydrogenated indium oxide. Appl Phys Express 8(1):015505
5. Kim H, Horwitz JS, Kushto G, Piqué A, Kafafi ZH, Gilmore CM, Chrisey DB (2000) Effect of film thickness on the properties of indium tin oxide thin films. J Appl Phys 88(10):6021–6025
6. Shigesato Y, Koshi-ishi R, Kawashima T, Ohsako J (2000) Early stages of ITO deposition on glass or polymer substrates. Vacuum 59(4):614–621
7. Sun XW, Huang HC, Kwok HS (1996) On the initial growth of indium tin oxide on glass. Appl Phys Lett 68(19):2663–2665
8. Yamada N, Yasui I, Shigesato Y, Li H, Ujihira Y, Nomura K (2000) Donor compensation and carrier-transport mechanisms in tin-doped In_2O_3 films studied by means of conversion electron ^{119}Sn Mössbauer spectroscopy and Hall effect measurements. Jpn J Appl Phys 39(7A):4158–4163
9. Martins R, Barquinha P, Pimentel A, Pereira L, Fortunato E (2005) Transport in high mobility amorphous wide band gap indium zinc oxide films. Phys Status Solidi A 202(9):R95–R97
10. Pödör B (1966) Electron mobility in plastically deformed germanium. Phys Status Solidi 16:K167
11. Utsuno F, Inoue H, Yasui I, Shimane Y, Tomai S, Matsuzaki S, Inoue K, Hirosawa I, Sato M, Honma T (2006) Structural study of amorphous In_2O_3 film by grazing incidence X-ray scattering (GIXS) with synchrotron radiation. Thin Solid Films 496(1):95–98

12. Buchholz DB, Zeng L, Bedzyk MJ, Chang RPH (2013) Differences between amorphous indium oxide thin films. Prog Nat Sci: Mate Int 23(5):475–480
13. Yamamoto T, Nomoto J, Kitami H, Sakemi T, Makino H, Kobayashi K, Aoki Y, Kishimoto S (2017) Design of advanced functional ZnO conductive thin films with arc plasma. J Vac Soc Jpn 60(8):292–299
14. Yamamoto T, Sakemi T, Awai K, Shirakata S (2004) Dependence of carrier concentrations on oxygen pressure for Ga-doped ZnO prepared by ion plating method. Thin Solid Films 451-452:439–442
15. Yamada T, Miyake A, Kishimoto S, Makino H, Yamamoto N, Yamamoto T (2007) Low resistivity Ga-doped ZnO thin films of less than 100 nm thickness prepared by ion plating with direct current arc discharge. Appl Phys Lett 91(5):051915
16. Nomoto J, Makino H, Yamamoto T (2016) High-Hall-mobility Al-doped ZnO films having textured polycrystalline structure with a well-defined (0001) orientation. Nanoscale Res Lett 11:320
17. Uramoto J, Ishii K, Kubota Y (1980) A disc LaB_6 cathode for plasma production in magnetic field. Research Report of Institute of Plasma Physics, Nagoya University. IPPJ, Japan, p 448
18. Yamamoto T, Song H, Makino H (2013) Effects of grain boundary scattering on carrier transport of highly transparent conductive Ga-doped ZnO polycrystalline films. Phys Stat Solidi C 10(4):603–606
19. Shirakata S, Sakemi T, Awai K, Yamamoto T (2006) Electrical and optical properties of large area Ga-doped ZnO thin films prepared by reactive plasma deposition. Superlattices Microstruct 39(1-4):218–228
20. Suzuki Y, Niino F, Katoh K (1997) Low-resistivity ITO films by dc arc discharge ion plating for high duty LCDs. J Non Cryst Solids 218:30–34
21. Sah RE, Driad R, Bernhardt F, Kirste L, Leancu C-C, Czap H, Benkhelifa F, Mikulla M, Ambacher O (2013) Mechanical and electrical properties of plasma and thermal atomic layer deposited Al_2O_3 films on GaAs and Si. J Vac Sci Technol A 31(4):041502–1-041502-7
22. Buchholz DB, Ma Q, Alducin D, Ponce A, Jose-Yacaman M, Khanal R, Medvedeva JE, Robert Chang RPH (2014) The Structure and Properties of Amorphous Indium Oxide. Chem Mat 26 (18):5401–5411
23. Kittel C (1996) Introduction to solid state physics, 7th edn. Wiley, New York, pp 158–159